Set Theoretic Localization of Fast Mobile Robots Using an Angle Measurement Technique

Uwe D. Hanebeck, Günther Schmidt

Department of Automatic Control Engineering
Technical University of Munich
D–80290 München, Germany

Abstract

We study the problem of localizing a mobile robot with an onboard–device making angular measurements on the location of known but undistinguishable landmarks. Novel algorithms are proposed for 1. efficient posture initialization based on a simple linear solution and for 2. recursive posture estimation. Derived in a set theoretic framework, the algorithms cope with nonwhite, nongaussian noise and deterministic errors. Experiments with the set theoretic posture estimator demonstrate its simplicity and effectiveness in real–world applications.

1 Introduction

This paper introduces a new view of estimating the absolute posture, i.e., position x, y, orientation ψ, of a fast mobile robot on a planar surface. The estimation is based upon onboard measurements of angular locations of known landmarks. Not only initialization of the robot posture, but also recursive in–motion posture estimation is considered.

For initialization purposes, a set of angles measured with respect to the robot coordinate system needs to be paired with a subset of the undistinguishable landmarks. In [1], an enumerative scheme has been reported for pairing the first three angles with landmarks. The remaining angles are used for plausibility tests. Several solutions for calculating the posture given the association of measured angles with landmarks have been reported: [1], [2], and [3] consider only triples of landmarks. For the case of more than three landmarks some authors average triple solutions, others use iterative techniques. [4] supplies a closed–form solution for N angles without considering uncertainties. In this paper, an efficient association algorithm is developed. It discards false measurements, is fast, and is further accelerated by incorporating prior knowledge. In addition, the algorithm takes advantage of a simple closed–form solution, which consists of a set of $N-1$ *linear* equations for the vehicle position, Sect. 3. An error propagation analysis considers uncertainties in both landmark positions and angle measurement.

Posture estimates are sequentially updated by newly incoming angle measurements, if the vehicle velocity is high compared to the angle measurement rate. The updates are usually performed within the Kalman filtering framework. White Gaussian zero-mean random processes are then used as uncertainty models. In [1], a Kalman filtering scheme is introduced for this purpose, which is based on a kinematic vehicle model; fusion of dead–reckoning information is not considered. [5] uses a Kalman filter to fuse sensor data with dead–reckoning data. Real–world uncertainties, however, also include nongaussian, nonwhite noise and systematic errors. These uncertainties may easily be considered in a set theoretic setting. For example, [6] describes a set theoretic approach to stereo vision based robot localization without dead–reckoning. In this paper, we solve the problem of locating a mobile robot based on onboard angle measurements in a set theoretic framework, Sect. 4. Basic concepts for prediction, measurement, and combination of information are developed from a set theoretic viewpoint in Sec. 4.1, Sec. 4.2, and Sec. 4.3 respectively. Section 4.3 then discusses two new approaches for 1. tailoring set theoretic estimators to specific applications, and for 2. achieving robustness against modeling errors. The individual components are tied together in Sec. 4.4 to construct a recursive set theoretic estimator with real–time capabilities. The benefits of the developed localization algorithm are demonstrated by experiments as discussed in Sect. 5. Combining set theoretic and Bayesian estimation is discussed in [7].

2 Problem Formulation

Consider a pool of M landmarks in a two–dimensional world or map. The positions of the landmarks $\underline{x}_i^{\text{LM}} = [x_i^{\text{LM}}, y_i^{\text{LM}}]^T$, $i = 0, 1, \ldots, M-1$ in a reference coordinate system are assumed to be known with additive bias errors $\underline{\Delta}_i^{\text{LM}} = [\Delta x_i^{\text{LM}}, \Delta y_i^{\text{LM}}]^T$, which are of course unknown. True values of $*$ are denoted as $\tilde{*}$, nominal values as $\hat{*}$. The true landmark position $\tilde{\underline{x}}_i^{\text{LM}}$ is assumed to lie somewhere within the set

$$\Omega_i^{\text{LM}} = \{\underline{x}_i^{\text{LM}} : \underline{x}_i^{\text{LM}} = \hat{\underline{x}}_i^{\text{LM}} + \underline{\Delta}_i^{\text{LM}}\,,\ \underline{\Delta}_i^{\text{LM}} \in \Omega_i^{\Delta}\}\ , \quad (1)$$

where the errors in the position of landmark i are confined to an ellipsoidal set Ω_i^{Δ} given by

$$\Omega_i^{\Delta} = \{\underline{\Delta}_i^{\text{LM}} : (\underline{\Delta}_i^{\text{LM}})^T (\mathbf{C}_i^{\text{LM}})^{-1} \underline{\Delta}_i^{\text{LM}} \leq 1\} . \quad (2)$$

Possible correlation of errors for different landmarks is ignored. The robot is capable of determining the angular locations of these landmarks with respect to its coordinate system. Individual landmarks do not necessarily have to be distinguished. The angle measurements are corrupted by additive noise, i.e., $\hat{\alpha}_i = \tilde{\alpha}_i + \Delta\alpha_i$, where $\Delta\alpha_i$ is assumed to be bounded in amplitude (b.i.a.) according to $|\Delta\alpha_i| < \delta_i^{\alpha}$.

To account for possible occlusion of landmarks in nonconvex rooms, partitioning walls are added to the map. The landmarks are ordered in the map in such a way, that the robot always detects the subset of unoccluded landmarks in that order when scanning counterclockwise.

3 Posture Initialization

This section is concerned with (re–) initializing the robot posture $\underline{x} = (x, y, \psi)^T$ in nonconvex rooms, when only very little prior knowledge is available. A priori information is specified by confining the posture to an ellipsoidal set $\Omega_{\text{a-priori}}$. M landmarks are available and $N > 3$ angles α_i, $i = 0, 1, \ldots, N-1$ have been measured. The association, i.e., the list of pairings of measured angles to landmarks is initially unknown. Inspired by the interpretation–tree (IT) method in [8], the association search is kept from becoming intractable by approaching it in two steps: In the first step, for every measured angle α_i the set of visible landmarks from $\Omega_{\text{a-priori}}$ is determined. In the second step, these visibility constraints are exploited for pruning the IT. Thus, only a small portion of all associations needs to be generated and tested.

Step 1: The projection of $\Omega_{\text{a-priori}}$ onto the x/y-plane is examined at polar grid points $x(r,\theta)$, $y(r,\theta)$ for some r, θ. We define a visibility matrix $\mathcal{V}$ with dimensions N by M. The elements $\mathcal{V}_{ij}$ are boolean variables which are TRUE, if the single measured angle α_i may be caused by landmark j. A visibility test is performed for every grid point $x(r,\theta)$, $y(r,\theta)$. If the landmark j is visible, i.e., when the straight line from the considered grid point $x(r,\theta)$, $y(r,\theta)$ to x_j^{LM}, y_j^{LM} does not intersect any partitioning walls, a hypothetical angle α_{hyp} is calculated. The minimum and maximum angles at $x(r,\theta)$, $y(r,\theta)$ within $\Omega_{\text{a-priori}}$ are denoted as ψ_{LOW}, ψ_{HIGH} respectively. α_i may then be caused by landmark j, if $\alpha_i + \psi_{\text{LOW}} < \alpha_{hyp} < \alpha_i + \psi_{\text{HIGH}}$. If row i of $\mathcal{V}$ does not contain any TRUE value, α_i has been identified as false measurement. Row i is then removed from $\mathcal{V}$ and the number of measurements N is decremented.

Step 2: Only those candidate associations are generated that do not violate the visibility constraints represented by $\mathcal{V}$ and that also follow the ordering assumption. Erroneous measurements are handled efficiently by adopting the "least bad data" constraint proposed in [9]. For a specific association, a tentative position is calculated and checked for compatibility with the error bounds, the posture constraint $\Omega_{\text{a-priori}}$, and the requirements for joint visibility of all landmarks involved.

Tentative postures are quickly calculated by use of a closed–form solution. The corresponding set of $N-1$ *linear* equations for the position is derived next. The measurement equation for a single angle measurement α_i is given by

$$\alpha_i = \text{atan2}(x_i^{\text{LM}} - x, y_i^{\text{LM}} - y) - \psi \ , \quad (3)$$

$i = 0, 1, \ldots, N-1$. Define γ_i as the difference between two consecutive angle measurements α_i and α_{i+1}

$$\begin{aligned} \gamma_i &= \alpha_{i+1} - \alpha_i \\ &= \text{atan2}(x_{i+1}^{\text{LM}} - x, y_{i+1}^{\text{LM}} - y) \\ &\quad - \text{atan2}(x_i^{\text{LM}} - x, y_i^{\text{LM}} - y) \ . \end{aligned} \quad (4)$$

Application of trigonometric identities leads to

$$\tan(\gamma_i) = \frac{\frac{y_{i+1}^{\text{LM}} - y}{x_{i+1}^{\text{LM}} - x} - \frac{y_i^{\text{LM}} - y}{x_i^{\text{LM}} - x}}{1 + \frac{y_{i+1}^{\text{LM}} - y}{x_{i+1}^{\text{LM}} - x} \cdot \frac{y_i^{\text{LM}} - y}{x_i^{\text{LM}} - x}} \ , \quad (5)$$

which may be rewritten as

$$\begin{aligned} & y_{i+1}^{\text{LM}} y_i^{\text{LM}} + x_{i+1}^{\text{LM}} x_i^{\text{LM}} + \cot(\gamma_i)\{x_{i+1}^{\text{LM}} y_i^{\text{LM}} - y_{i+1}^{\text{LM}} x_i^{\text{LM}}\} \\ &= \begin{bmatrix} \cot(\gamma_i)\{y_i^{\text{LM}} - y_{i+1}^{\text{LM}}\} + x_{i+1}^{\text{LM}} + x_i^{\text{LM}} \\ \cot(\gamma_i)\{x_{i+1}^{\text{LM}} - x_i^{\text{LM}}\} + y_{i+1}^{\text{LM}} + y_i^{\text{LM}} \end{bmatrix}^T \begin{bmatrix} x \\ y \end{bmatrix} \\ &\quad - [x \quad y] \begin{bmatrix} x \\ y \end{bmatrix} \end{aligned} \quad (6)$$

for $i = 0, 1, \ldots, N-1$. Index operations are performed modulo N, i.e., $i+1 = 0$ for $i = N-1$. Subtracting from every equation its follower equation yields a system of $N-1$ equations that are *linear* in x and y, i.e.,

$$\underline{z} = \mathbf{H}\,[x, y]^T + \underline{e} \quad (7)$$

with

$$\begin{aligned} \underline{z} &= [z_0, z_1, \ldots, z_{N-2}]^T \\ \mathbf{H} &= [\underline{h}_0, \underline{h}_1, \ldots, \underline{h}_{N-2}]^T \\ \underline{h}_i &= [h_i^x, h_i^y]^T \end{aligned} \quad (8)$$

and error $\underline{e} = [e_0, e_1, \ldots, e_{N-2}]^T$. The corresponding

elements are given by

$$
\begin{aligned}
z_i &= y_{i+1}^{\mathrm{LM}} y_i^{\mathrm{LM}} + x_{i+1}^{\mathrm{LM}} x_i^{\mathrm{LM}} - y_{i+2}^{\mathrm{LM}} y_{i+1}^{\mathrm{LM}} - x_{i+2}^{\mathrm{LM}} x_{i+1}^{\mathrm{LM}} \\
&\quad + \cot(\gamma_i)\{x_{i+1}^{\mathrm{LM}} y_i^{\mathrm{LM}} - y_{i+1}^{\mathrm{LM}} x_i^{\mathrm{LM}}\} \\
&\quad - \cot(\gamma_{i+1})\{x_{i+2}^{\mathrm{LM}} y_{i+1}^{\mathrm{LM}} - y_{i+2}^{\mathrm{LM}} x_{i+1}^{\mathrm{LM}}\} \\
h_i^x &= \cot(\gamma_i)\{y_i^{\mathrm{LM}} - y_{i+1}^{\mathrm{LM}}\} + x_i^{\mathrm{LM}} \\
&\quad - \cot(\gamma_{i+1})\{y_{i+1}^{\mathrm{LM}} - y_{i+2}^{\mathrm{LM}}\} - x_{i+2}^{\mathrm{LM}} \\
h_i^y &= \cot(\gamma_i)\{x_{i+1}^{\mathrm{LM}} - x_i^{\mathrm{LM}}\} + y_i^{\mathrm{LM}} \\
&\quad - \cot(\gamma_{i+1})\{x_{i+2}^{\mathrm{LM}} - x_{i+1}^{\mathrm{LM}}\} - y_{i+2}^{\mathrm{LM}} \ .
\end{aligned}
\tag{9}
$$

Once x, y are known, ψ can be obtained as the (weighted) LS–solution of (3) for $i = 0, 1, \ldots, N-1$. An error propagation analysis is performed, which provides 1. the optimal weighting matrix for the LS–solution of (7) and 2. the initial set of postures that are compatible with the a priori error bounds. This analysis is found elsewhere.

4 Recursive In–Motion Localization

Once the robot posture is initialized using the method developed in the last section, the robot may start moving. During motion, the robot posture estimate is updated with the information obtained from every single angle measurement. A dead–reckoning system is used to smooth the estimate by predicting the posture change between two measurements.

Usually, problems of this type are solved within the Kalman filter framework. Measurement noise and dead–reckoning errors are assumed to be zero–mean, white, mutually independent random processes. For these assumptions, the Kalman prediction step (time update) provides first and second order moments of the predicted state given *any* noise distribution. The Kalman estimation step (measurement update), however, yields precise values of first and second order moments of the estimated state only for Gaussian noise densities. For any other noise density, the Kalman estimation step just represents the best *linear* estimator.

In practical applications, however, a state estimator must cope with 1. nongaussian noise densities, 2. nonwhite noise, 3. systematic errors, and 4. mutally dependent noise sources. For the localization problem at hand, at least two error sources may be identified, that violate the Kalman filter assumptions:

1. landmark positions are only known within a deterministic offset, and
2. a robot's dead–reckoning system — especially for the omnidirectional robot considered in Sec. 5 — suffers from nonwhite noise and deterministic errors.

A nonlinear filter, which copes with the above mentioned uncertainties, is developed by set theoretic considerations in the following. The proposed filter is first order for the sake of simplicity, i.e, strictly optimal for white b.i.a. noise processes. However, the output represents an upper bound for nonwhite noise or deterministic errors, which is in sharp contrast to first order Kalman filters. Furthermore, the noise processes may stem from *any* distribution that is compatible with the amplitude bounds.[1] Ellipsoidal bounding sets (EBS) are used to approximate the sets of feasible solutions. They may be manipulated by matrix operations only, which leads to efficient algorithms with real–time capabilities.

Section 4.1 develops a simple method for set theoretic posture prediction. The determination of the set of feasible postures defined by a single angle measurement is discussed in Sec. 4.2. An efficient algorithm for approximating the intersection of prediction and measurement set is introduced in Sec. 4.3. These three filtering components are put together in Sec. 4.4 to form a nonlinear recursive set theoretic estimator.

4.1 Set Theoretic Posture Prediction

When moving from one measurement at time $k-1$ to the next, the vehicle posture suffers from accumulating uncertainties. The relative uncertainty may be estimated and must then be "added" to the absolute uncertainty prevalent at time $k-1$. Usually, the relative uncertainty is assumed to be independent from the absolute uncertainty at time $k-1$, which leads to the well known Kalman covariance propagation formula. For nonwhite noise and deterministic errors, however, this propagation formula is too optimistic. In the following, a simple set theoretic propagation formula is developed, that provides a guaranteed upper bound for the posture error even in the case of nonwhite and deterministic errors.

The result of the fusion process at time $k-1$ is denoted as Ω_{k-1}^E and given by

$$
\Omega_{k-1}^E = \{\underline{x}_{k-1}^E : (\underline{x}_{k-1}^E - \hat{\underline{x}}_{k-1}^E)^T \left(\mathbf{C}_{k-1}^E\right)^{-1} (\underline{x}_{k-1}^E - \hat{\underline{x}}_{k-1}^E) \leq 1\}. \tag{10}
$$

The dead–reckoning system supplies the set of relative postures with respect to Ω_{k-1}^E, henceforth denoted as

$$
\Omega_k^\Delta = \{\underline{x}_k^\Delta : (\underline{x}_k^\Delta - \hat{\underline{x}}_k^\Delta)^T \left(\mathbf{C}_k^\Delta\right)^{-1} (\underline{x}_k^\Delta - \hat{\underline{x}}_k^\Delta) \leq 1\} \ . \tag{11}
$$

The calculation of Ω_k^Δ depends on the vehicle kinematic. For the omnidirectional vehicle considered in Sec. 5, determining Ω_k^Δ is rather complex and outside the scope of this paper.

The exact set of absolute postures is given by transforming the set Ω_k^Δ to the inertial coordinate system

[1] Not only uniform densities !

for all feasible posture estimates contained in Ω_{k-1}^E. This is written as

$$\Omega_k^P = \{\underline{x}_k^P : \underline{x}_k^P = \mathbf{I}\,\underline{x}_{k-1}^E + \mathbf{B}_k\,\underline{x}_k^\Delta\}\ , \qquad (12)$$

with $\underline{x}_{k-1}^E \in \Omega_{k-1}^E$, $\underline{x}_k^\Delta \in \Omega_k^\Delta$, $\mathbf{I}$ the identity matrix, and

$$\mathbf{B}_k = \begin{bmatrix} \cos(\psi_{k-1}^E) & -\sin(\psi_{k-1}^E) & 0 \\ \sin(\psi_{k-1}^E) & \cos(\psi_{k-1}^E) & 0 \\ 0 & 0 & 1 \end{bmatrix}\ . \qquad (13)$$

Unfortunately, Ω_k^P is not in general an ellipsoid. Linearizing (12) around the nominal values yields

$$\underline{x}_k^P - \hat{\underline{x}}_k^P \approx \mathbf{J}_k^E(\underline{x}_{k-1}^E - \hat{\underline{x}}_k^E) + \hat{\mathbf{B}}_k(\underline{x}_k^\Delta - \hat{\underline{x}}_k^\Delta) \qquad (14)$$

with the Jacobian

$$\mathbf{J}_k^E = \begin{bmatrix} 1 & 0 & -(\hat{y}_k^P - \hat{y}_{k-1}^E) \\ 0 & 1 & (\hat{x}_k^P - \hat{x}_{k-1}^E) \\ 0 & 0 & 1 \end{bmatrix}\ . \qquad (15)$$

Ω_k^P may then be approximated as the EBS for the Minkowski sum of the two ellipsoids in (14)

$$\Omega_k^P \approx \{\underline{x}_k^P : (\underline{x}_k^P - \hat{\underline{x}}_k^P)^T \left(\mathbf{C}_k^P\right)^{-1} (\underline{x}_k^P - \hat{\underline{x}}_k^P) \le 1\}\ , \qquad (16)$$

with center $\hat{\underline{x}}_k^P$ and $\mathbf{C}_k^P$ given by

$$\hat{\underline{x}}_k^P = \mathbf{I}\,\hat{\underline{x}}_{k-1}^E + \hat{\mathbf{B}}_k\,\hat{\underline{x}}_k^\Delta\ ,\ \mathbf{C}_k^P = \frac{\mathbf{\Xi}_k}{0.5-\kappa} + \frac{\mathbf{\Gamma}_k}{0.5+\kappa}\ , \qquad (17)$$

with $\mathbf{\Xi}_k = \mathbf{J}_k^E \mathbf{C}_{k-1}^E (\mathbf{J}_k^E)^T$, $\mathbf{\Gamma}_k = \hat{\mathbf{B}}_k \mathbf{C}_k^\Delta \hat{\mathbf{B}}_k^T$, for $-0.5 < \kappa < 0.5$.[2] κ may be selected such that a measure of the "size" of Ω_k^P is minimized.

4.2 Posture Set Defined by Measurement

The measurement equation for a single α_k at time k and an associated landmark at $\underline{x}^{\mathrm{LM}}$ is given by (3) and may be rewritten as

$$\begin{aligned} &\sin(\alpha_k + \psi_k^M)\{x^{\mathrm{LM}} - x_k^M\} \\ &= \cos(\alpha_k + \psi_k^M)\{y^{\mathrm{LM}} - y_k^M\}\ . \end{aligned} \qquad (18)$$

Linearizing around the predicted posture $\hat{\underline{x}}_k^P$, the measured angle $\hat{\alpha}_k$, and the nominal landmark position $\hat{\underline{x}}^{\mathrm{LM}}$ yields the measurement set

$$\Omega_k^M = \{\underline{x}_k^M : z_k = \underline{H}_k^T \underline{x}_k^M + e_k\ ,\ e_k^2 \le E_k\}\ . \qquad (19)$$

z_k, $\underline{H}_k$, and E_k are derived in the appendix.

[2] $-0.5 < \kappa < 0.5$ leads to symmetric solution formulae for κ in contrast to the formulation in [10], that assumes $0 < \kappa < 1$.

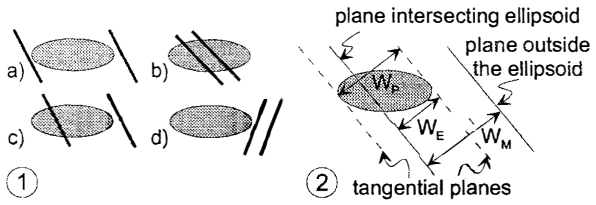

Figure 1: 1: Configurations for measurement strip and prediction ellipsoid (2D). 2: Definitions for assessing consistency of the two sets.

4.3 Robust Combination of Information

After measurement k, the vehicle posture simultaneously belongs to two sets: 1. the prediction set Ω_k^P, which carries all past information from dead-reckoning and previous measurements, and 2. the measurement set Ω_k^M, which accounts for the last angle measurement. Consequently, fusion consists of calculating the intersection of the two sets Ω_k^P, Ω_k^M. However, the intersection of Ω_k^P and Ω_k^M is not in general again an ellipsoid. Thus, an ellipsoid circumscribing the intersection is required to arrive at a recursive scheme. A bounding ellipsoid is given by [11]

$$\begin{aligned} \Omega_k^E &= \{\underline{x}_k^E : (\underline{x}_k^E - \hat{\underline{x}}_k^E)\left(\mathbf{C}_k^E\right)^{-1}(\underline{x}_k^E - \hat{\underline{x}}_k^E)^T \le 1\} \\ \mathbf{C}_k^E &= d_k \mathbf{D}_k \\ \mathbf{D}_k &= \mathbf{C}_k^P - \lambda_k \frac{\mathbf{C}_k^P \underline{H}_k \underline{H}_k^T \mathbf{C}_k^P}{E_k + \lambda_k G_k} \\ \hat{\underline{x}}_k^E &= \hat{\underline{x}}_k^P + \lambda_k \mathbf{D}_k \underline{H}_k E_k^{-1} \epsilon_k \\ \epsilon_k &= z_k - \underline{H}_k^T \hat{\underline{x}}_k^P \\ G_k &= \underline{H}_k^T \mathbf{C}_k^P \underline{H}_k \\ d_k &= 1 + \lambda_k - \lambda_k \epsilon_k^2/(E_k + \lambda_k G_k) \end{aligned} \qquad (20)$$

for all $\lambda_k \ge 0$. The set Ω_k^E possesses the interesting property that it both contains the intersection of the measurement and the prediction set and is itself contained in their union, i.e.,

$$(\Omega_k^M \cap \Omega_k^P) \subset \Omega_k^E \subset (\Omega_k^M \cup \Omega_k^P)\ . \qquad (21)$$

Furthermore, the set Ω_k^E is valid for any noise distribution complying with the amplitude bounds. But more importantly, no independence assumption is used in the derivation. As a result, the estimator provides a reliable uncertainty quantification even in the case of nonwhite or deterministic measurement errors.

Although very similar in appearance to the Kalman filter equations [3], (20) defines a nonlinear estima-

[3] In fact, for $\lambda_k = 1$ and $d_k = 1$, (20) yields the Kalman filter equations, when $\mathbf{C}_k^E$, $\mathbf{C}_k^P$, and E_k are interpreted as covariance matrices.

tor which inherits a selective update mechanism. The nonlinear estimator comprises the following cases:

- **Consistency:** Prediction set Ω_k^P and measurement set Ω_k^M possess common points.
  - **Full consistency:**
    - **No uncertainty reduction:** The actual measurement is of no help in reducing the uncertainty, Fig 1.1 a).
    - **Uncertainty reduction:** Both planes defining the measurement set intersect the ellipsoidal prediction set, Fig. 1.1 b).
  - **Partial consistency:** Only one plane intersects the prediction set, Fig. 1.1 c).
- **Inconsistency:** Prediction set Ω_k^P and measurement set Ω_k^M do not share a common point, Fig. 1.1 d).

Inconsistency is detected by checking the condition

$$d_k(\lambda_k^{\min}) < 0 \ , \quad \text{with } \lambda_k^{\min} = \sqrt{\frac{E_k}{G_k}} \ . \tag{22}$$

No update is then performed. For the case of **consistency** of ellipsoid and strip, the *volume* of the bounding ellipsoid in (20) may be minimized by selecting the weight λ_k^{OPT} as the most positive root of the quadratic equation given by [11]

$$\begin{aligned}&\lambda_k^2(N-1)G_k^2 + \lambda_k\{\epsilon_k^2 + (2N-1)E_k - G_k\}G_k \\ &+\{N(E_k - \epsilon_k^2) - G_k\}E_k = 0 \ ,\end{aligned} \tag{23}$$

where N is the dimension, here $N = 3$. The case of no uncertainty reduction is characterized by $\lambda_k^{\text{OPT}} \leq 0$.

Ellipsoidal Bounding Set with Minimum Volume Projection Onto Subspace

For the considered application, it is more natural to minimize the volume of the projection of the EBS onto the x, y subspace. The EBS with a *minimum volume projection* onto an arbitrary subspace is obtained with λ_k^{OPT} as the positive real root of

$$\begin{aligned}&\lambda_k^3(G_k - K_k)G_k^2 L + \lambda_k^2\{L(3G_k - 2K_k) - K_k\}E_k G_k \\ &+ \lambda_k\{\epsilon_k^2(L(K_k - G_k) + K_k) + E_k(L(3G_k - K_k) - K_k) \\ &- G_k K_k\}E_k + \{L(E_k - \epsilon_k^2) - K_k\}E_k^2 = 0 \ ,\end{aligned} \tag{24}$$

with L the subspace dimension and

$$K_k = \underline{H}_k^T(\bar{\mathbf{C}}_k^P)^T[\text{proj}(\mathbf{C}_k^P)]^{-1}\bar{\mathbf{C}}_k^P\underline{H}_k \ . \tag{25}$$

$\bar{\mathbf{C}}_k^P$ is obtained from $\mathbf{C}_k^P$ by eliminating the rows not associated with the considered subspace. The proof is patterned after the one in [12] and is sketched in the appendix. Application to the localization problem leads to a tailor–made bounding operation. The inherently high precision of the orientation estimate ψ_k^E compared to the position estimate x_k^E, y_k^E is considered by minimizing the projection of the EBS onto the x, y subspace. The resulting EBS is more conservative in ψ_k^E, but tight for the more critical position estimate x_k^E, y_k^E.

Robust Fusion

Using the "smallest" EBS is successful as long as the model is sufficiently precise. However, modeling errors may lead to an unreasonably small estimation set Ω_k^E. Enhanced robustness is achieved by imposing a higher priority on the set of predicted states Ω_k^P since it contains all past information. This priority should depend on the degree of consistency of the two sets Ω_k^P and Ω_k^M. Roughly speaking, the idea is to select the set Ω_k^E such that it exhibits a growing tendency towards the prediction set Ω_k^P with falling degree of consistency of the sets Ω_k^P and Ω_k^M. Referring to Fig. 1.2, a reasonable consistency measure is given by the intersection width W_k^E divided by the geometric mean of the strip width W_k^M and the ellipsoid width W_k^P

$$\text{CM}(\Omega_k^P, \Omega_k^M) = \frac{W_k^E}{\sqrt{W_k^P W_k^M}}, \ 0 \leq \text{CM} \leq 1 . \tag{26}$$

λ_k in (20) is selected from $[0, \lambda_k^{\text{OPT}}]$ as an appropriate function of the consistency measure. For this purpose, a shifted logistic function

$$\lambda_k = \lambda_k^{\text{OPT}}/[1 + \exp(-S(\text{CM} - M))] \ , \tag{27}$$

is used with $S = 10$, $M = 0.5$. The influence of this extension on the fusion result is demonstrated in Fig. 2 by comparing it with the common approach for four cases. For the common approach, the volume of the resulting EBS Ω_k^E experiences large changes when the measurement set just changes slightly. Single (unmodeled) measurement outliers may lead to an extremely small EBS. On the other hand, the new approach calculates Ω_k^E by modifying Ω_k^P depending on its consistency with Ω_k^M. Thus, single erroneous measurements have a reduced impact on the fusion result. The volume of the EBS as a function of d, where d is the distance of the ellipsoid center from the strip center axis, is shown for this example in Fig. 3.

Remark: The smallest possible EBS is obtained from (20) when both hyperplanes defining Ω_k^M intersect Ω_k^P. Overbounding occurs when one of the hyperplanes falls outside Ω_k^P. The minimum volume bounding ellipsoid would then be obtained by parallel repositioning of the outside plane to be tangential to Ω_k^P [13]. This is not exploited here, since overbounding is intentionally performed in the case of partial consistency by using consistency measures.

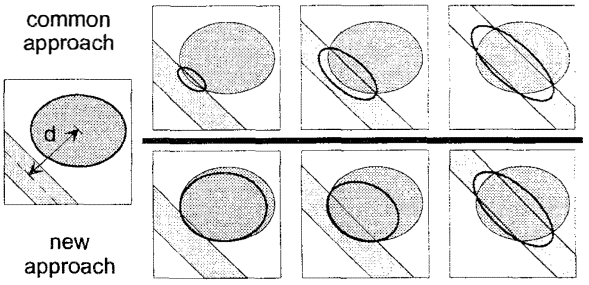

Figure 2: EBSs for the intersection of ellipsoid and strip. Top: Common scheme. Bottom: Extension employing consistency measures.

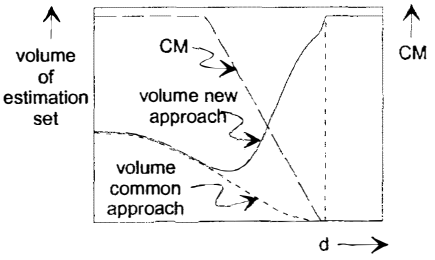

Figure 3: Volume of the EBS in Fig. 2.

4.4 Set Theoretic Recursive Estimator

The proposed recursive estimation scheme for localization during fast motion is depicted in Fig. 4. Based on the set of estimated postures Ω_{k-1}^E at time $k-1$, the visible landmarks are determined and validation bounds for a measured angle are predicted. If the actual measured angle falls outside of these bounds, it is discarded. Otherwise, it is associated with the best matching landmark and the measurement strip Ω_k^M is calculated. Ω_k^M is then fused with the set of predicted postures Ω_k^P to produce Ω_k^E. The feedback of $\hat{\underline{x}}_k^E$ to the process for determination of Ω_k^M deserves some attention. It replaces $\hat{\underline{x}}_k^P$ for iterative refinement of the linearization of (18). For implementation purposes, the scheme has been parallelized into three tasks: The fusion loop, the determination of landmarks not occluded by partitioning walls, and dead–reckoning.

5 Experimental Validation

The effectiveness of the new approach is demonstrated by navigating the fast (2 m/sec) omnidirectional service robot ROMAN (ROving MANipulator) [14] through an office environment. ROMAN is a full scale mobile robot adapted to indoor requirements: width 0.63 m x depth 0.64 m x height 1.6 m. Three independently steerable wheel systems provide excellent maneuverability. Wheel diameters of 0.2 m allow travel across rough surfaces like carpeted floor. For absolute localization of ROMAN, an onboard laser–based goniometer is used. An eye–safe laser beam scans the environment in a horizontal plane and determines the azimuth angles to known artificial landmarks, i.e., retro–reflecting tape strips attached to the walls. To keep the hardware simple, no distance information is supplied and the landmarks are not distinguished. 20 horizontal 360°–scans per second are performed; absolute accuracy is about 0.02°. A map contains nominal positions of 34 identical landmarks and partitioning walls, Fig. 6. Landmark positions have been aquired by the robot itself during an exploration trip. The dead–reckoning system employs the robot's odometry and a gyroscope. Odometry is based on the drive wheels and suffers from error sources like imperfect wheel coordination and uncertain wheel/floor contact points. The gyroscope suffers from a slowly time–varying unknown offset.

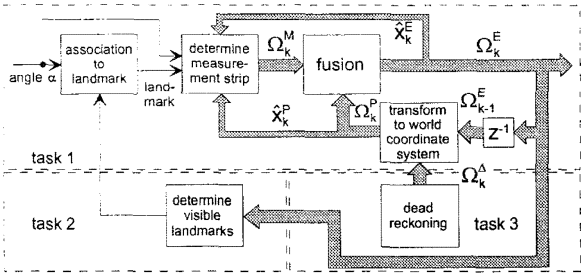

Figure 4: Scheme of set theoretic recursive estimator.

Once initialized, the robot repetetively travels along the predefined course depicted in Fig. 6. The total distance travelled is about 650 m, the total time is 35 min. The maximum speed is 1000 mm/sec, and the average speed is 312 mm/sec. The robot passes four doorways at each loop, two of which are narrow (80 cm, robot width is 63 cm). The localization estimate based on the fusion of goniometer data and dead–reckoning is compared for the first two loops with data from dead–reckoning only. The highly correlated nature of the accumulating dead–reckoning errors is obvious. On the other hand, the vehicle is kept accurately on track by means of the localization estimate. Absolute deviation has found to be about ±2 cm and ±0.5° for the low–speed passages and about ±5 cm and ±1° for the high–speed passages.

The localization system is now in operation for more than one year and serves as the basis for research on mobile manipulation tasks. It has been extensively tested by covering a distance of more than a hundred kilometers. Experiments include long–range navigation like the one discussed above, door opening/passing maneuvers, and high–speed runs with maximum velocities of up to 2 m/sec. Set theoretic estimation proved to be an appropriate alternative to

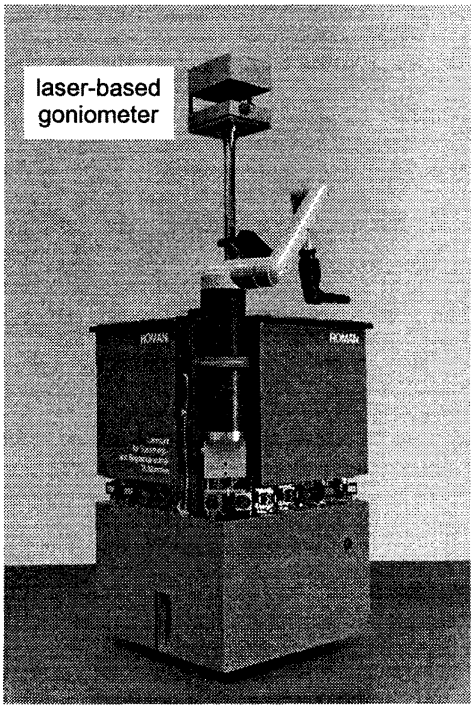

Figure 5: Omnidirectional mobile manipulator.

the common statistical approaches when dealing with strongly correlated or deterministic uncertainties.

6 Conclusion

Set theoretic concepts have been applied to posture estimation of fast–moving mobile robots which perform angular measurements on the location of known landmarks. The landmarks do not need to be distinguished by the robot. Four main results have been presented:
1. an efficient algorithm for posture initialization in nonconvex rooms,
2. a simple *closed–form* solution for the robot position given angular locations of N known landmarks, which consists of $N-1$ equations *linear* in the position,
3. an extension of the common minimum volume EBS algorithms to obtain the EBS with *minimum volume projection* onto an arbitrary subspace, and
4. a new design approach for set theoretic estimators which employs consistency measures to achieve robustness against modeling errors.
The effectiveness of the proposed set theoretic estimator has been demonstrated by experiments with a fast omnidirectional service robot. The full scale robot is equipped with a laser–based goniometer which makes angular measurements on the location of tape strips attached to the wall as artificial landmarks. Navigation in an office environment revealed a maximum deviation of about ± 5 cm and $\pm 1^0$ between true and estimated robot location.

Acknowledgement: The work reported in this paper was supported by the Deutsche Forschungsgemeinschaft as part of an interdisciplinary research project on "Information Processing Techniques in Autonomous Mobile Robots" (SFB 331).

References

[1] U. Wiklund, U. Andersson, and K. Hyyppä, "AGV Navigation by Angle Measurements", *Proc. of the 6th Int. Conf. on Automated Guided Vehicle Systems, Brussels, Belgium*, pp. 199–212, 1988.

[2] K. T. Sutherland and W. B. Thompson, "Localizing in Unstructured Environments: Dealing with the Errors", *IEEE Trans. on Robotics and Automation*, vol. 10, no. 6, pp. 740–754, 1994.

[3] T. Tsumura, H. Okubo, and N. Komatsu, "A 3-D Position and Attitude Measurement System Using Laser Scanners and Corner Cubes", *Proc. of the 1993 IEEE/RSJ Int. Conf. on Intelligent Robots and Systems, Yokohama, Japan*, pp. 604–611, 1993.

[4] M. Betke and L. Gurvits, "Mobile Robot Localization Using Landmarks", *Proc. of the 1994 IEEE/RSJ/GI Int. Conf. on Intelligent Robots and Systems, Munich, Germany*, pp. 135–142, 1994.

[5] T. Nishizawa, A. Ohya, and S. Yuta, "An Implementation of On–board Position Estimation for a Mobile Robot", *Proc. of the 1995 IEEE Int. Conf. on Robotics and Automation, Nagoya, Japan*, pp. 395–400, 1995.

[6] S. Atiya and G. D. Hager, "Real–Time Vision Based Robot Localization", *IEEE Trans. on Robotics and Automation*, vol. 9, no. 6, pp. 785–800, 1993.

[7] U. D. Hanebeck, J. Horn, and G. Schmidt, "On Combining Set Theoretic and Bayesian Estimation", *Proc. of the 1996 IEEE Int. Conf. on Robotics and Automation, Minneapolis, MN, this issue*, 1996.

[8] M. Drumheller, "Mobile Robot Localization Using Sonar", *IEEE Trans. on PAMI*, vol. 9, no. 2, pp. 325–332, 1987.

[9] W. E. L. Grimson and T. Lozano-Pérez, "Recognition and Localization of Overlapping Parts From Sparse Data in Two and Three Dimensions", *Proc. of the 1985 IEEE Int. Conf. on Robotics and Automation, St. Louis, MO*, pp. 61–66, 1985.

[10] F. C. Schweppe, *Uncertain Dynamic Systems*, Prentice–Hall, 1973.

[11] A. Sabater and F. Thomas, "Set Membership Approach to the Propagation of Uncertain Geometric Information", *Proc. of the 1991 IEEE Int. Conf. on Robotics and Automation, Sacramento, CA*, pp. 2718–2723, 1991.

[12] J. R. Deller Jr and T. C. Luk, "Linear Prediction Analysis of Speech Based on Set–Membership Theory", *Computer Speech and Language*, vol. 3, pp. 301–327, 1989.

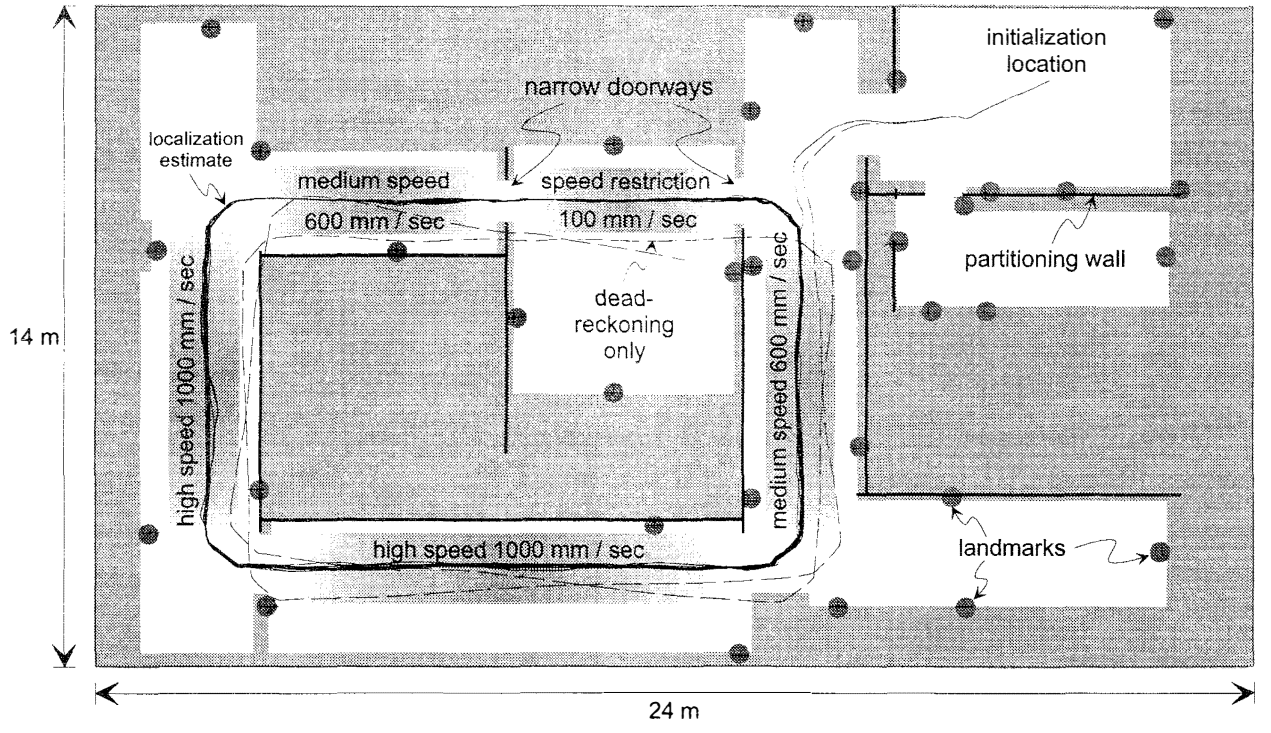

Figure 6: Result of continuous long–range navigation.

[13] M.-F. Cheung *et al.*, "An Optimal Volume Ellipsoid Algorithm for Parameter Set Identification", *IEEE Trans. on AC*, vol. 38, no. 8, pp. 1292–1296, 1993.

[14] U. D. Hanebeck and G. Schmidt, "A New High Performance Multisonar System for Fast Mobile Robots", *Proc. of the 1994 IEEE/RSJ/GI Int. Conf. on Intelligent Robots and Systems, Munich, Germany*, pp. 1853–1860, 1994.

7 Appendix

The coefficients of (19) are given by

$$\begin{aligned} z_k &= c_k^1 \hat{x}^{\text{LM}} - c_k^2 \hat{y}^{\text{LM}} - c_k^3 \hat{\psi}_k^P \\ \underline{H}_k &= [c_k^1, -c_k^2, -c_k^3]^T \\ e_k &= [-c_k^1, c_k^2][\Delta x^{\text{LM}}, \Delta y^{\text{LM}}]^T - c_k^3 \Delta\alpha_k \ . \end{aligned} \tag{28}$$

The constants are defined as $c_k^1 = \sin(\hat{\alpha}_k + \hat{\psi}_k^P)$, $c_k^2 = \cos(\hat{\alpha}_k + \hat{\psi}_k^P)$, and $c_k^3 = c_k^2\{\hat{x}^{\text{LM}} - \hat{x}_k^P\} + c_k^1\{\hat{y}^{\text{LM}} - \hat{y}_k^P\}$. e_k can thus be bounded, i.e.,

$$|e_k| \leq \sqrt{\begin{bmatrix} -c_k^1 \\ c_k^2 \end{bmatrix}^T \mathbf{C}^{\text{LM}} \begin{bmatrix} -c_k^1 \\ c_k^2 \end{bmatrix}} + |c_k^3| \delta_k^\alpha \ . \tag{29}$$

Proof of (24): The projection of $\mathbf{C}_k^E$ onto a certain subspace is denoted as $\text{proj}(\mathbf{C}_k^E)$ and may be written as

$$d_k \,\text{proj}(\mathbf{C}_k^P) - \lambda_k d_k \frac{\text{proj}(\mathbf{C}_k^P \underline{H}_k \underline{H}_k^T \mathbf{C}_k^P)}{E_k + \lambda_k G_k} \ . \tag{30}$$

The volume of $\text{proj}(\mathbf{C}_k^E)$ is proportional to

$$\det\left(d_k \mathbf{I} - \lambda_k d_k \frac{[\text{proj}(\mathbf{C}_k^P)]^{-1} \bar{\mathbf{C}}_k^P \underline{H}_k \underline{H}_k^T (\bar{\mathbf{C}}_k^P)^T}{E_k + \lambda_k G_k} \right) , \tag{31}$$

where $\bar{\mathbf{C}}_k^P$ is defined as $\mathbf{C}_k^P$ with those rows eliminated, that are not associated with the considered subspace. Applying the matrix identity [12]

$$\det(c\mathbf{I} + \underline{y}\underline{z}^T) = c^{L-1}(c + \underline{y}^T \underline{z}) \ , \tag{32}$$

where L is the subspace dimension, (31) becomes

$$d_k^L \frac{E_k + \lambda_k (G_k - K_k)}{E_k + \lambda_k G_k} \ , \tag{33}$$

with K_k from (25). Differentiating with respect to λ_k and setting the result to zero yields (24).